Journal of
Materials Chemistry C

Accepted Manuscript

This article can be cited before page numbers have been issued, to do this please use: T. Tang, T. T. Lin, F. Erden, F. Wang and C. He, *J. Mater. Chem. C*, 2018, DOI: 10.1039/C8TC00895G.

ROYAL SOCIETY
OF CHEMISTRY

rsc.li/materials-c

View Article Online
DOI: 10.1039/C8TC00895G

Journal Name

ARTICLE

Configurations dependent optical properties and acid susceptibility of azulene compounds

Received 00th January 20xx,
Accepted 00th January 20xx

DOI: 10.1039/x0xx00000x

www.rsc.org/

Tao Tang,[a,b] Tingting Lin,[b] Fuat Erden,[a,b] Fuke Wang,*[b] and Chaobin He*[a, b]

We report the unique optical and protonation characteristics of azulene compounds with different molecular configurations, and demonstrate their potential application as acid sensor materials. The unique characteristic of azulene compound is its large dipole moment, and azulene derivatives with conjugation either along or orthogonally to the dipole direction of azulene were synthesized and their electronic and optical properties were studied. Our results showed that azulene with conjugation orthogonally to the dipole direction exhibits significantly optical properties change upon protonation due to strong intermolecular charge transfer. The low band gap absorption can reach up to mid-IR range, albeit at high acid doping concentration. On the other hand, conjugated azulenes along the dipole direction could be protonated easily even at very low acid concentration (ppm level), which is attributed to the co-planar structures upon protonation and their high proton affinity. Mechanism behind the discrepancy between the two configurations are elucidated and further supported by computer simulation. The application of azulene chromophore for chemical sensor with sensitivity at ppm level was also demonstrated in this work.

Introduction

Azulene is the best known nonalternant aromatic hydrocarbon for its large dipole moment and unusual excited state properties.[1-3] The absolute values of atomic orbital coefficients for azulene indicate that the electrons in the highest occupied molecular orbital (HOMO) and the lowest unoccupied molecular orbital (LUMO) have relatively little overlap, particularly at the nodal points of C2 and C6 in HOMO and C1 and C3 in LUMO (Scheme 1a).[4-6] This leads to a relatively small electron repulsion energy in the first excited singlet state and thus a low transition energy to the S1 state in the visible region. The large dipole moment (1.08 D) of azulene arises from the fusion of the electron-rich five-membered ring (cyclopentadienyl anion) and the electron-poor seven-membered ring (electron tropylium cation), resulting in the electron drift from the seven-membered ring to five-membered ring. This unique configuration of azulene makes it an ideal building block for designing functional molecules with direction-dependent property. That is, the optical band gap and on-off fluorescence could be easily modulated using different substitution patterns either along or orthogonally to the dipole direction of azulene (Scheme 1b).

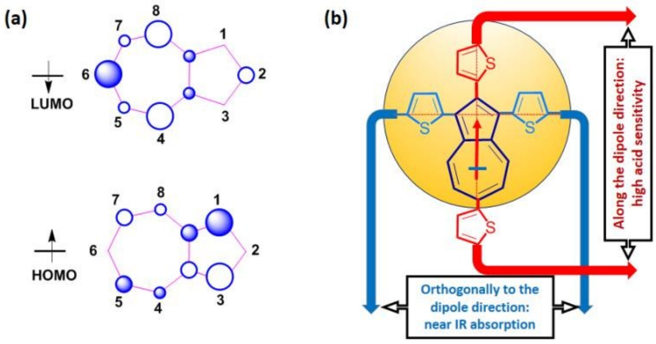

Scheme 1 (a) The relative electron density of the HOMO and LUMO of azulene ring. (b) Molecular design of azulene derivatives with conjugation either along or orthogonally to the dipole direction of azulene.

To date, azulene-based conjugated materials have been reported for many applications such as conducting polymers,[7-10] near IR absorption,[11, 12] fluorescent switching,[13, 14] electrochromic devices,[15-17] and organic solar-cell materials.[18-20] In most of these functional materials, azulene was used as core building block through the conjugation along the C1-C3 direction (orthogonally to the dipole direction of azulene) due to their facile synthesis, pH-responsive behavior and interesting optical properties. Particularly, we have reported a series of near and middle IR responsive polymers in the range of 800 nm to 2.5 μm for applications in near IR absorption and electrochromic devices (ECDs).[12] These azulene-containing

---

[a] *Department of Materials Science and Engineering, National University of Singapore, 9 Engineering Drive 1, Singapore 117576.*
[b] *Soft Materials Department, Institute of Materials Research and Engineering, Agency for Science, Technology and Research (A*STAR), 2 Fusionopolis Way, #08-03 Innovis, Singapore 138634.*
*Email - wangf@imre.a-star.edu.sg

Electronic Supplementary Information (ESI) available: [details of any supplementary information available should be included here]. See DOI: 10.1039/x0xx00000x

View Article Online
DOI: 10.1039/C8TC00895G

polymers were prepared through coupling at C1 and C3 of azulene, and they could be protonated using high concentration of organic acid such as trifluoroacetic acid (TFA). The near-IR absorption was attributed to the protonation-induced intramolecular charge transfer (ICT) transition. On the other hand, as shown in Scheme 1a, C2-C6 conjugated connection (along the dipole direction of azulene) of azulene is expected to be more interesting than other configurations because the high symmetry of C_{2v} can be retained in the C2-C6 coupled of azulene structures. As a result, the electrons could be delocalized on dipolar C_{2v} axis of azulene and thus leads to a large hyperpolarizability and a large dipole moment, which takes full advantage of azulene structure.[13] However, due to long and elaborate synthetic procedures, it is only recently that the C2-C6 conjugated coupled azulene chromophores were successfully synthesized.[21-24] These C2-C6 conjugated azulene oligomers showed strong intermolecular interactions and high-order orientations in crystalline state, together with tunable-polarity FET characteristic.[22, 23] It is also reported that the C2-C6 linked polyaminoazulene showed good proton conductivity.[24] While azulene-based materials with C1-C3 and C2-C6 conjugation have been reported respectively, the exploration of the unique characteristics of azulene compounds conjugated at either C1-C3 or C2-C6 positions for practical application has not been reported.

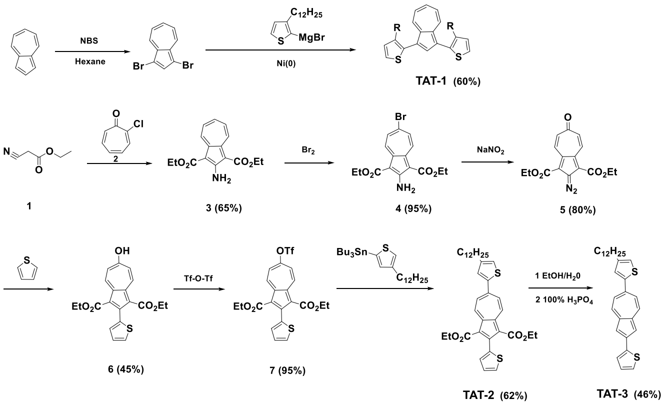

Scheme 2 The synthesis of the conjugated compounds.

We here report the synthesis and optical studies of azulene-thiophene oligomers coupled at either C1-C3 or C2-C6 directions (Scheme 1b), and their unusual optical properties upon protonation were also compared. We showed that the large polar azulene core induced a strong intermolecular charge transfer upon protonation, leading to a remarkable red shift to near IR absorption upon protonation, albeit at high acid concentration; while a high sensitivity to ppm level of acid was achieved for the azulene-thiophene oligomer coupled along the C2-C6 direction, which was attributed to the co-planar structures upon protonation and their high proton affinity. To the best of our knowledge, this is the first to report the unique different characteristics of azulene compounds with conjugation at different positions. Moreover, this works represents the first study on stimuli-responsive behavior of C2-C6 conjugated azulene compounds in both solution and the solid state. The mechanism behind is also elucidated, and their application as ultra-sensitive acid sensor materials is demonstrated.

Results and discussion

Synthesis and characterization

The general synthetic procedure for the molecules is shown in Scheme 2. The coupling reaction between ethyl cyanoacetate (**1**) and 2-chlorocyclohepta-2,4,6-trien-1-one (**2**) gave the product diethyl 2-aminoazulene-1,3-dicarboxylate (**3**). Bromination of diethyl 2-aminoazulene-1,3-dicarboxylate (**3**) in solution of chloroform gave compounds 2-amino-6-bromo-azulene-1,3-dicarboxylic acid diethyl ester (**4**). Successively, diazotization of compound **4** in synthesis of 2-diazo-6-oxo-2,6-dihydro-azulene-1,3-dicarboxylic acid diethyl ester (**5**) was conducted in TFA under 0 °C. Photochemical reaction of compound **5** in thiophene generated diethyl 6-hydroxy-2-(thiophen-2-yl)azulene-1,3-dicarboxylate (**6**). Diethyl 2-(thiophen-2-yl)-6-(((trifluoromethyl)sulfonyl)oxy)azulene-1,3-dicarboxylate (**7**) was obtained through reacting compound **6** with triflic anhydride. The Stille coupling reaction between compound **7** and tributyl(4-dodecylthiophen-2-yl)stannane were carried out to give compound diethyl 6-(4-dodecylthiophen-2-yl)-2-(thiophen-2-yl)azulene-1,3-dicarboxylate (**TAT-2**) in good yield (0.25g, 62%). Finally, compound **8** (0.5 g) was dealkoxycarboxylated by hydrolysis in ethanol/water and then in H_3PO_4 at 130 °C to give 4-dodecyl-2-(2-(thiophen-2-yl)azulen-6-yl)thiophene (**TAT-3**). **TAT-1** containing 1,3-connected azulene is also synthesized as control group to compared with **TAT-2** and **TAT-3** containing 2,6-connected azulene. The chemical structures of new compounds were identified by ^{1}H NMR, ^{13}C NMR and HRMS (ESI †).

Protonation studies

As shown in Fig. 1, UV-vis spectra of **TAT**s demonstrate absorption bands in the region $\lambda < 600$ nm. The absorption maxima for **TAT-1** is 306 nm. TD-DFT calculation reproduces well with the spectrum of **TAT-1** ($\varepsilon = 5.6 \times 10^4$ M cm^{-1}). The shoulder in 343 and 423 nm is ascribed to the HOMO→LUMO+1, HOMO-1→LUMO and HOMO-3→LUMO transitions. Bathochromic shift is observed when C1-C3 connectivity of azulene in **TAT-1** is changed to C2-C6 connected azulene in **TAT-2** and **TAT-3**. Both **TAT**-2 and **TAT-3** exhibit dual-band absorption. The low energy absorption band and high energy absorption band are attributed to the charge transfer and π-π* transition, respectively. Azulene itself possesses a D-A structure with electron drifting from the seven-membered ring to the five-membered ring. Therefore, conjugation connection of azulene along its dipole direction (C2-C6) reinforced the hyperpolarizability and dipole moment along the molecule backbone, and thus leads to charge separation and red-shifted absorption. Therefore, the maximum absorption for **TAT-2** (ε =

View Article Online
DOI: 10.1039/C8TC00895G

8.1×10^4 M cm^{-1}) and **TAT-3** ($\varepsilon = 1.01 \times 10^5$ M cm^{-1}) shifted to 464 and 439 nm, respectively.

Remarkable spectral change is observed upon protonation. The longest bathochromic shift is found for **TAT-1**. **TAT-1** shows newly formed high-energy absorption band (460 – 780 nm) and low-energy absorption band (850 – 1400 nm) upon protonation, which is comparable to our previous results.[25,26] On the other hand, **TAT-3** exhibits a distinct absorption band with high molar extinction coefficient (547 nm) in comparison with **TAT-1** and **TAT-2**. The measured molar extinction coefficients for protonated compounds **TAT-1** at 1125 nm are 0 (1% TFA), 5.3×10^3 (10% TFA) and 4.01×10^4 M cm^{-1} (30% TFA). **TAT-3** demonstrates the molar extinction coefficient of 1.09×10^5 M cm^{-1} when TFA concentration is 1%. However, **TAT-2** does not display obvious spectral change upon the protonation process, which was attributed to the scarce electron density at the five-membered ring of azulene in **TAT-2**. It is well known that electron-rich position with high proton affinity is important for the protonation.[27,28] Alkoxycarboxylated group may greatly reduce electron density of the five-membered ring of azulene. Reduced electron density and steric hindrance thus inhibit the protonation of azulene in **TAT-2**.

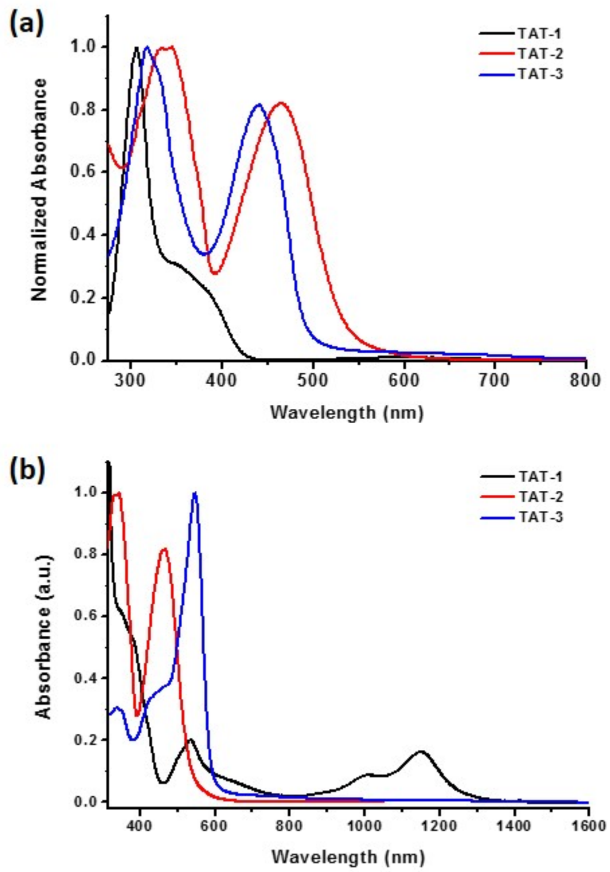

Fig. 1 Normalized optical absorption spectra of **TAT**s in $CHCl_3$ solution (a) before and (b) after protonation with TFA.

The UV-vis-NIR spectra change for both **TAT-1** and **TAT-3** under different TFA concentration are studied. In general, an increase of TFA concentration leads to the increased intensity of newly formed absorption bands and bleaching of original π-π* transition. Although both chromophores are responsive to TFA, their sensitivities to acid is quite different. Remarkable spectra change for **TAT-1** can only be observed when TFA concentration was above 3% (V). Also, when the TFA concentration was beyond 30% (V), the spectra change becomes unnoticeable again, suggesting an acidic saturation is reached at this TFA concentration.[12,25] Interestingly, **TAT-3** shows an ultra-sensitivity to acid as compared to **TAT-1**. As can be seen in Fig. 2, trace amount of TFA (0.07% v/v) can induce significant spectral change, and the acid saturation reached at low TFA concentration (~1% (v/v)). An isosbestic point observed at 475 nm is consistent with two inter-converting optically different phases being present in the solution. Moreover, these acid-mediated optical changes of **TAT-3** are reversible in solution, with original spectral characteristics by being recovered after neutralization of the protonated species using triethylamine. This protonation-deprotonation process can be repeated for more than 20 times without remarkable spectra change.

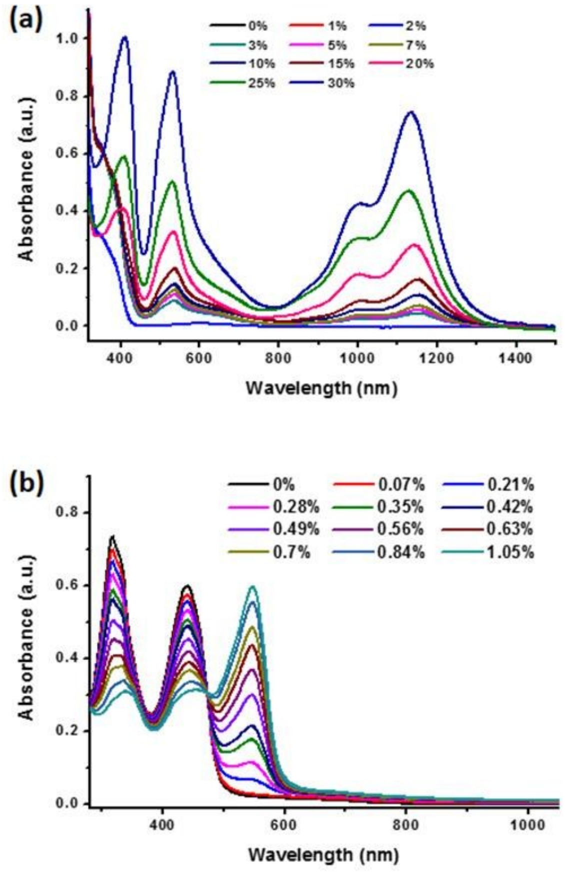

Fig. 2 UV-vis-NIR spectra of the chloroform **TAT-1** (a) and **TAT-3** (b) in chloroform solution as a function of TFA concentration.

The protonated azulenes also demonstrate interesting emissive properties. Neutral **TAT**s in $CHCl_3$ do not show any detected fluorescence. However, upon protonation, **TAT-1** and **TAT-3** give emissive spectra with λ_{max} at 460 and 580 nm, respectively (Fig. 3). Similar to their absorption spectra, the

View Article Online
DOI: 10.1039/C8TC00885G

fluorescence intensities of **TAT-1** and **TAT-3** vary with TFA concentrations. For example, the fluorescence intensity of **TAT-3** reaches to the highest point at TFA concentration of 0.033% (v/v). The relative fluorescence efficiencies (ϕ_f) of **TAT-1** and **TAT-3** in $CHCl_3$ were measured by using quinine sulphate and Rhodamine B as standard. The measured ϕ_fs of **TAT-1** and **TAT-3** were at 0.006 and 0.04 in $CHCl_3$/TFA, respectively. The emission intensity of **TAT-3** is more than 6 times higher than **TAT-1** which could be attributed to the co-planar electronic structures of protonated **TAT-3** as will be discussed below.

All these results suggest that both the C1-C3 and C2-C6 conjugated azulenes showed reversible protonation-deprotonation process. However, due to the different electronic configuration, their spectra change upon protonation and sensitivity to acid are significantly different. These spectra and sensitivities change make azulenes versatile materials. The spectra change upon protonation allows the design of absorption materials covering from visible to IR ranges. For instance, the C2-C6 conjugated azulene help to cover the visible range while the C1-C3 conjugated azulene will cover the near IR spectra range. On the other hand, the sensitivity difference makes it possible to design sensors that are applicable both in the low and high acid concentration range (from ppm level to high concentrated). The remarkably different spectra change upon protonation is further elucidated in the following DFT calculation, and the highly sensitivity of C2-C6 conjugated **TAT-3** was attributed to the high proton affinity (PA) of the C1 and C3 position in azulene. The computer calculated PA for the **TAT-1** and **TAT-3** were found to be 254.4 and 267.7 ha, respectively.

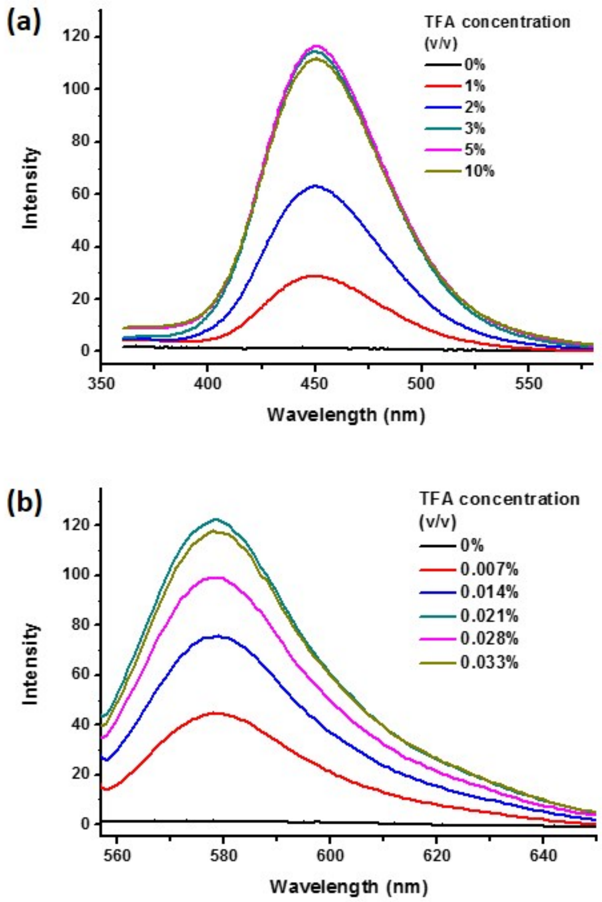

Fig. 3 Fluorescence spectra of (a) **TAT-1** and (b) **TAT-3** in the presence of TFA. The excited wavelengths (λ_{ex}) are 360 and 545 nm, for **TAT-1** and (b) **TAT-3**, respectively.

Computer simulation studies

In order to clarify the absorption difference between **TAT-1** and **TAT-3**, DFT calculation is conducted. The geometry optimisation and energy calculations were performed with Gaussian 09 software suite using B3LYP/6-31+G(d,p) (Fig. 4).[29] For simplification, the long alkyl chains were replaced with methyl groups. For neutral **TAT-1**, HOMO is delocalized on the whole backbone, while LUMO is located on azulene. After protonation, HOMO is mainly distributed on thiophene units while LUMO is delocalized on protonated azulene. For neutral **TAT-3**, both HOMO and LUMO are delocalized on the whole backbone. Upon protonation, HOMO is delocalized on the whole backbone while LUMO is located on protonated azulene and part of thiophene units.

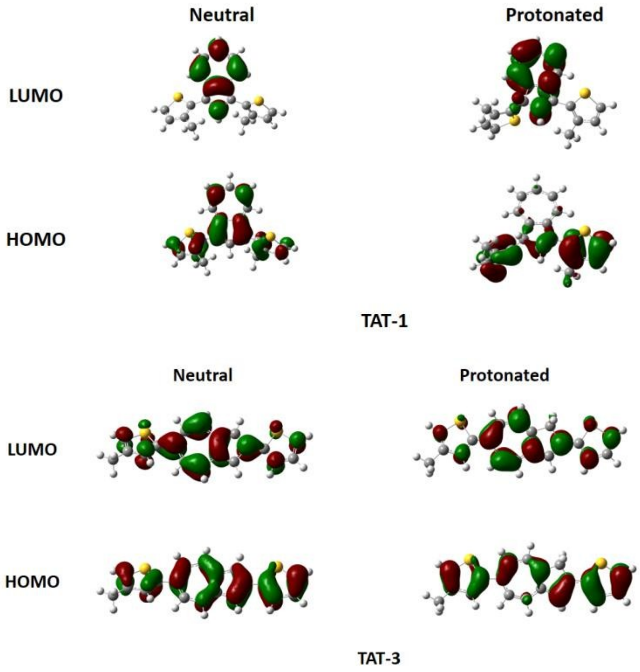

Fig. 4 Optimized structures of frontier molecular orbitals for model compounds **TAT-1** and **TAT-3** in their neutral and protonated states (green and red lobes indicate orbital lobes).

Computer simulation indicated that the charge separation for protonated **TAT-1** is more efficient than that for protonated **TAT-3**, thus leads to a greater reduction of band-gap and more red-shifted absorption of protonated **TAT-1**. Moreover, dipole moment for protonated **TAT-1** (7.34 D) is four times larger than that of protonated **TAT-3** (1.82 D) which may be due to the twisted donor/acceptor in protonated **TAT-1**. Fig. 5 shows the simulated electrostatic potential (ESP) map of the protonated **TAT-1** and **TAT-3** where the proton was added to C-1 of azulene.

View Article Online
DOI: 10.1039/C8TC00895G

Clearly, we can see that the positive charge is mainly delocalized on the seven-membered ring of azulene in protonated **TAT-1** while the positive charge is delocalized on the whole molecule in protonated **TAT-3**. The conformational analysis of both protonated molecules were displayed in Fig. 5, where the relative energy of the molecular as function of the torsion angle between thiophene and azulene ring was calculated using DFT theory. Protonated **TAT-1** and **TAT-3** showed significant different stable states of molecular conformation. For protonated **TAT-1**, the low energy conformation was found at large twisted angles between azulene and thiophene rings, while for protonated **TAT-3**, the stable state was found at the co-planar conformation. Meanwhile, TD-DFT is also done to calculate the excited states for molecules. For neutral **TAT-3**, 453.9 (oscillation strength, f = 1.0576) and 303.7 nm (f = 1.0351) are the main absorption bands. Upon the protonation, simulation shows main absorption bands are 505.3 (f = 1.1928) and 401.2 nm (f = 0.2085). The TD-DFT further validates the UV-vis spectra of molecules.

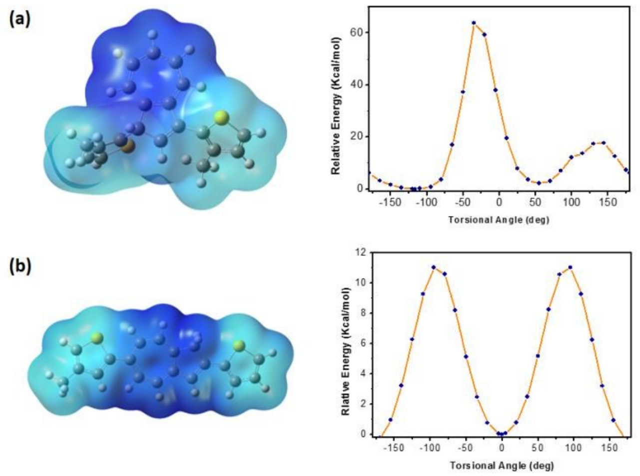

Fig. 5 The comparison of the electrostatic potential (ESP) mapping of protonated (a) **TAT-1** and (b) **TAT-3**. The right curve show the conformational analysis of both protonated molecules as function of the torsion angle between thiophene and azulene ring.

Applications in TFA sensing

TAT-3 showed much higher sensitivity to low TFA concentration at ppm level, in contrast to **TAT-1**. Furthermore, solid **TAT-3** film showed even higher sensitivity to TFA. The compound films were prepared via dip-coating the **TAT-3** solution onto TLC plate and then dried under atmosphere. Fig. 6 shows the color change of **TAT-3** film when exposure to TFA at various gas concentrations. The original plate showed a light yellow color. Upon the addition of 10 ppm TFA, the plate color became darker in seconds. At higher TFA concentration (> 30 ppm), the color changed from dark yellow to pink. A bright-pink color can be observed when TFA concentration was higher than 50 ppm. These results suggest that **TAT-3** shows a higher sensitivity to TFA at solid state than in solution. Moreover, similar response could also be observed in the fluorescence change. Under the same situation, solid **TAT-3** film gave stronger red light when TFA concentration gradually increases (Supporting Information). Most importantly, solid **TAT-3** film displayed reversible color change (either in absorption or emission). The solid film can be easily protonated by TFA vapour, and recovered to its original color upon treatment with ammonium or argon gas flow. The reversibility and durability of the colorimetric response of **TAT-3** to TFA was investigated by monitoring the color change upon repeating the protonation-deprotonation process for many consecutive cycles as shown in Fig. 6. Digital photographs of the film over the course of the cycling experiment were subjected to a colorimetric evaluation in RGB (red, green, blue) color levels based on literatures.[30] Color change in form of green channel as a function of cycle number is displayed in Fig. 6b, where good reversibility and durability of the protonation and deprotonation process can be observed.

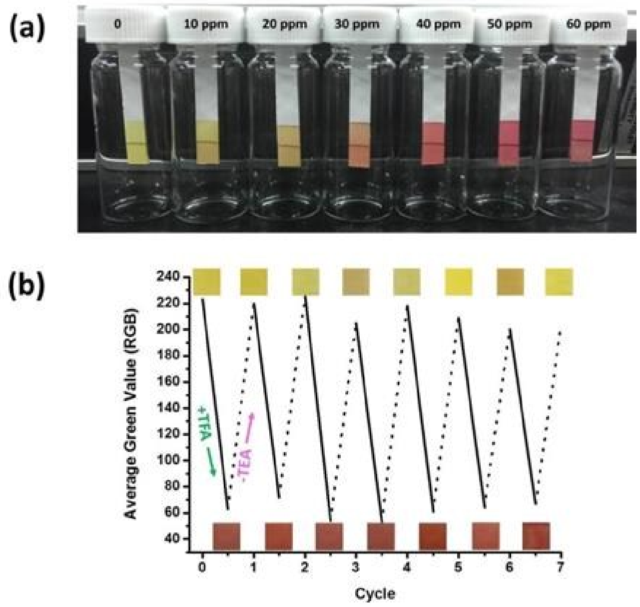

Fig. 6 (a) Color change of TAT-3 film when exposure to various TFA concentration. (b) RGB color analysis (green channel) of the reversible protonation/deprotonation of a thin film of **TAT-3** over 7 complete cycles (exposure to TFA vapor followed by removal of TFA under a flow of argon). The colored squares above and below the data points are actual images of the thin film at each step.

Conclusions

In summary, we here reported the synthesis and optical studies of azulene derivatives with different electronic configurations. Our results showed that the C1-C3 conjugated azulenes displaying a remarkable spectra shift to near IR range upon protonation due to strong ICT effect, but they are less sensitive to acid concentration as remarkable spectra revolution can only be observed at high TFA concentration (> 3%, v/v). However, the C2-C6 conjugated azulenes showed less spectra shift upon protonation, but they are extremely sensitive to TFA. Obviously

View Article Online
DOI: 10.1039/C8TC00895G

spectra change can be observed at low TFA concentration (ppms), particularly for the solid state **TFA-3** film. These differences were illustrated by DFT simulation and the application for TFA sensing was demonstrated with good reversibility and durability. These results suggest that azulene is a versatile building unit for molecular design to achieve various applications, simply by tuning the molecular electronic configuration.

Experimental details

Materials

Ethyl cyanoacetate (98%), 2-chlorocyclohepta-2,4,6-trien-1-one (98%), thiophene (99%), triethylamine (99%) lithium chloride (99%), trifluoroacetic acid (99%), triphenylarsine (97%) and trifluoromethanesulfonic anhydride (99%) were purchased from Sigma-Aldrich. Dichloromethane (CH_2Cl_2) was distilled with calcium hydride to remove water. Other commercially available solvents and reagents were used as received.

Instrumentation

^{1}H-NMR (400.13 MHZ) and ^{13}C-NMR (100.61 MHZ) spectra were recorded on Bruker DRX 400-MHZ NMR spectrometer in the solvent of $CDCl_3$ at room temperature. Tetramethylsilane (TMS) was used as an internal standard to express chemical shift. Mass spectra were measured on a Bruker micrOTOFQII. UV-vis-NIR spectra were conducted on Agilent Cary 5000. Fluorescence Spectroscopy was conducted on RF-5301PC of Shimadzu. The monomer solution is dip-coated on TLC glass plate. The monomer on substrate was sealed with various TFA concentrations in provided sample holder with a quartz cover.

Simulation

All calculations were performed with the Gaussian 09 program employing the Becke Three Parameter Hybrid Functionals Lee−Yang−Parr (B3LYP) in conjunction with the 6-31+G(d,p) basis set.[26] Full geometry optimizations without symmetry constraints were carried out in the gas phase for the singlet ground states (S_0). The energies of highest occupied molecular orbital (HOMO), lowest unoccupied molecular orbital (LUMO) and other frontier orbitals were calculated at the optimized structure. In all cases, the normal modes revealed no imaginary frequencies indicating that they represent minima on the potential energy surface.

Synthesis of compounds

*Diethyl 2-aminoazulene-1,3-dicarboxylate (**3**)*. In the RBF equipped with thermometer and additional funnel placed about 6 ml anhydrous ethanol and then 0.13 g sodium metal was added. After the sodium was dissolved, the reaction flask was put into an ice-water bath. Then 0.67 ml ethyl cyanoacetate (**1**) was added slowly. After the addition was finished, solution of 2-chlorocyclohepta-2,4,6-trien-1-one (2, 0.4 g, 2.84 mmol) in anhydrous ethanol was added drop by drop and the solution was changed to yellow immediately after the addition. The reaction continued at 5-10 °C for another 4 hours, followed by quench of reaction via adding 25 ml water and extraction with $CHCl_3$. The volatile was removed through rotary evaporator. The crude product was chromatographed on silica gel using hexane/ethyl acetate (4/1, v/v) as eluent to afford the title compound (65 %) as light brown solids. ^{1}H-NMR (δ, $CDCl_3$): 9.15 (d, 2 H, J = 10.8 Hz), 7.80 (m, 2 H), 7.55 (t, 2 H, J = 10.8 Hz), 7.44 (t, 1 H, J = 8.4 Hz), 4.46 (q, 4 H), 1.48 (t, 6 H).

*2-Amino-6-bromo-azulene-1,3-dicarboxylic acid diethyl ester (**4**).* Diethyl 2-aminoazulene-1,3-dicarboxylate (**3**, 0.1 g, 0.35 mmol) and 2 ml chloroform were added into 25 ml flask. After all the materials dissolved, 0.06 g bromine dissolved in 0.5 ml chloroform was added and reacted overnight. A dark orange solution was obtained and then poured into water. Then the reaction was extracted with CH_2Cl_2 (15 ml x 3). The organic layers were combined and washed with 20 ml $NaHCO_3$ solution (three times), 30 ml water (three times) and dried over magnesium sulfate. After filtration, the volatile $CHCl_3$ and CH_2Cl_2 were removed through rotary evaporator. The crude product was chromatographed on silica using hexane/ethyl acetate (5/1, v/v) as eluant. This was obtained as orange solid (95%). ^{1}H-NMR (δ, $CDCl_3$): 8.76 (d, 2 H, J = 11. 2 Hz), 7.77 (m, 2 H), 7.75 (d, 2 H, J =11.2 Hz), 4.56 (q, 4 H), 1.47 (t, 6 H).

*2-Diazo-6-oxo-2,6-dihydro-azulene-1,3-dicarboxylic acid diethyl ester (**5**)*. The 2-amino-6-bromo-azulene-1,3-dicarboxylic acid diethyl ester (**4**, 0.4 g, 1.09 mmol) was dissolved in 4 ml TFA at 0 °C. The mixture was degassed by Ar. $NaNO_2$ (0.25 g, 3.6 mmol) was added in portions over 10 mins under Ar. Then the reaction was stopped by addition of water and extracted with $CHCl_3$ (15 ml x 3). The organic layers were combined and washed with NaOH solution, 30 ml water (three times) and dried over magnesium sulfate. After filtration, the volatile $CHCl_3$ was removed through rotary evaporator. The crude product was chromatographed on silica gel using hexane/ethyl acetate (2/1, v/v) as eluant. This was obtained as bright yellow solid (80%). ^{1}H-NMR (δ, $CDCl_3$): 8.35 (d, 2 H, J = 12.3 Hz), 6.66 (d, 2 H, J= 12.2 Hz), 4.44 (m, 4 H), 1.44 (m, 6 H). ^{13}C NMR: δ 189.5, 161.5, 133.6, 133.1, 131.6, 120.8, 61.6, 14.0. HRMS(APCI): calcd for $C_{16}H_{14}N_2O_5$, m/z 314.0903; found, m/z 314.1056.

*Dethyl 6-hydroxy-2-(thiophen-2-yl)azulene-1,3-dicarboxylate (**6**)*. Thiophene (500 ml) was first degassed with Ar for about 4 hours and then transferred into a quartz reaction tube charged with 2-diazo-6-oxo-2,6-dihydro-azulene-1,3-dicarboxylic acid diethyl ester (**5**, 1 g, 2.70 mmol). The reaction tube was put into a UV-reactor equipped with the 3000Å UV lamp. After overnight reaction, the thiophene was removed and the residue was purified by column chromatography on silica gel using hexane/ethyl acetate (1/1, v/v) as eluent, affording the desired product as yellow solid (45%). ^{1}H-NMR (δ, $CDCl_3$): 9.36 (d, 2 H, J= 11.2 Hz), 7.38 (m, 1 H), 7.29 (m, 2 H), 7.11 (m, 2 H), 6.97 (m, 2 H), 4.16 (m, 4 H), 1.06 (m, 6 H). ^{13}C NMR: δ 168.9, 166.5, 142.3, 139.1, 138.9, 137.6, 127.0, 126.0, 125.2, 119.6, 118.2, 60.3, 13.6. HRMS(APCI): calcd for $C_{20}H_{18}N_4O_5S$, m/z 370.0875; found, m/z 370.0976.

*Diethyl 2-(thiophen-2-yl)-6-(((trifluoromethyl)sulfonyl)oxy)azulene-1,3-dicarboxylate (**7**)*. Dethyl 6-hydroxy-2-(thiophen-2-yl)azulene-1,3-dicarboxylate (**6**, 0.37 g, 1 mmol) was suspended on 20 ml anhydrous CH2Cl2. The mixture was cooled down to -20 °C by dry ice-acetone bath under Ar. Et_3N (0.42 ml, 3 mmol) was added drop by drop and form a clear red-orange solution. Then triflic anhydride (0.25 ml, 1.5 mmol) was added via syringe slowly. After the addition, the reaction was maintained at -20 °C for 10 mins. TLC showed all the starting materials has been converted to the products. Then the reaction was stopped by addition of water and extracted with $CHCl_3$ (15 ml x 3). The organic layers were combined and washed with $NaHCO_3$ solution, 30 ml water (three times) and dried over magnesium sulfate. After filtration, the volatile $CHCl_3$ was removed through rotary evaporator. The crude product was chromatographed on silica gel using hexane/ethyl acetate (2/1, v/v) as eluant. This was obtained as bright yellow solid (80%). ^{1}H-NMR (δ, $CDCl_3$): 9.48 (d, 2 H, J =11.44 Hz), 7.58 (d, 2 H, J = 11.16 Hz), 7.48 (d, 2 H, J= 4.12 Hz), 7.10 (m, 2 H), 4.23 (m, 4 H), 1.09 (t, 6 H, J = 7.08 Hz). ^{13}C NMR: δ 164.9, 155.7, 148.2, 140.3, 136.8, 136.5, 128.2, 126.7, 126.3, 123.5, 122.7, 60.6, 13.7. HRMS(APCI): calcd for $C_{21}H_{17}F_3O_7S_2$, m/z 502.0368; found, m/z 502.0674.

*1,3-Bis[2-(3-n-dodecylthienyl)]azulene (**TAT-1**)*. To a round bottom flask added magnesium turning (37.5 mmol) and anhydrous THF (30 ml). Under argon protection, a solution of 2-bromo-3-dodecylthiophene in anhydrous THF (10 ml) was added dropwise with stirring. After finishing the addition, the resulting mixture was stirred at room temperature for 1 hour and then reflux for 4 hours until all magnesium turnings were disappeared. The formed Grignard reagent was then transferred to mixture of 1,3-dibromoazulene (6 mmol) and Ni(dppp)Cl_2 (0.22 g) in anhydrous THF that has been cooed in ice-water bath. After all Grignard reagent was transferred, the reaction mixture was then warm to room temperature and reflux overnight. The mixture was cooled down to room temperature and then dilute HCl solution (200 ml) was added under stirring. The organic layer was separated and the aqueous layer was extract with ether for 3 times. Combined the organic layers and washed with sodium bicarbonate solution, water, and brine successively. It was dried over magnesium sulfate and purified by chromatography on silica gel using hexane as eluant. The product was dark green oil (60%). ^{1}H-NMR (δ, $CDCl_3$): 8.36 (d, 2H, J = 9.64 Hz), 7.92 (s, 1H), 7.61 (t, 1H, J = 9.76 Hz), 7.34 (d, 2H, J = 5.24 Hz), 7.16 (t, 2H, J = 9.84 Hz), 7.09 (d, 2H, J = 5.16 Hz), 2.56 (t, 4H, J = 7.56 Hz), 1.52 (m, 4H), 1.22 (m, 36H), 0.87 (t, 6H, J = 5.32 Hz).

*Diethyl 6-(4-dodecylthiophen-2-yl)-2-(thiophen-2-yl)azulene-1,3-dicarboxylate (**TAT-2**)*. To a 3-necked 100 ml RBF was added LiCl (84 mg, 1.98 mmol), AsPh3 (0.202 g, 0.66 mmol), Pd(PPh3)4 (76.2 mg, 0.066 mmol) and diethyl 2-(thiophen-2-yl)-6-(((trifluoromethyl)sulfonyl)oxy)azulene-1,3-dicarboxylate (7, 0.33g, 0.66 mmol). The RBF was connected to a vacuum pump and then flashed with Ar. After repeating 3 times, 15 ml degassed 1,4-dioxane was added under Ar. Tributyl(4-dodecylthiophen-2-yl)stannane (0.36 g, 0.66 mmol) was added via syringe and the mixture then reacted at 80 °C for 8 hours. Upon the check with TLC, the reaction mixture was first diluted with ethyl acetate and then 8 ml of saturated KF aqueous solution was added to precipitate the excess tin reagents. The organic volatile was removed through rotary evaporator. The crude product was chromatographed on silica gel using hexane/ethyl acetate (4/1, v/v) as eluent to afford brown solid (62%). ^{1}H-NMR (δ, $CDCl_3$): 9.46 (d, 2 H, J = 11.08 Hz), 7.81 (d, 2 H, J = 11.12 Hz), 7.43 (m, 1 H), 7.40 (m, 1 H), 7.11-7.05 (m, 3 H), 4.21 (m, 4 H), 2.72 (t, 2 H, J = 7.84 Hz), 1.63 (m, 4 H), 1.33 (m, 16 H), 1.04 - 0.87 (m, 9 H). ^{13}C NMR: δ 146.9, 146.1, 141.0, 139.0, 138.3, 138.0, 129.5, 128.1, 127.8, 127.5, 126.5, 126.2, 125.0, 119.3, 60.5, 32.1, 31.0, 30.8, 30.1, 29.4, 28.2, 27.2, 23.0, 17.9, 14.5, 14.1, 14.0. HRMS(APCI): calcd for $C_{36}H_{44}O_4S_2$, m/z 604.2681; found, m/z 604.2943.

View Article Online
DOI: 10.1039/C8TC00895G

*4-Dodecyl-2-(2-(thiophen-2-yl)azulen-6-yl)thiophene (**TAT-3**)*. To a 1-necked 50 ml RBF was added diethyl 6-(4-dodecylthiophen-2-yl)-2-(thiophen-2-yl)azulene-1,3-dicarboxylate (**TAT-2**, 500 mg, 0.8 mmol), 20 ml ethanol and 14 ml 2M KOH solution. The mixture was refluxed overnight. Upon cooling, the 20 ml 1M HCl solution was added to acidify the mixture. The precipitated crystals were collected by filtration, washed with water, and dried in vacuo.

A mixture of above product (438 mg, 0.8 mmol) and freshly prepared 100% phosphoric acid, which was obtained by dissolving phosphorus pentaoxide (1.28 g) in 85% phosphoric acid (3.2 g), was heated at 130 °C for 10 min with occasional stirring with a glass rod. After the reaction mixture was cooled, the mixture was poured into ice-water and extracted with $CHCl_3$. The organic layer was washed with water, dried over MgSO4, and concentrated via rotary evaporator. The crude product was chromatographed on silica gel using hexane/ $CHCl_3$ (1/2, v/v) as eluent to afford green solid (46%). ^{1}H-NMR (δ, $CDCl_3$): 8.16 (d, 2 H, J = 10.68 Hz), 7.57-7.50 (m, 5 H), 7.34 (m, 2 H), 7.12 (m, 1 H), 7.00 (s, 1 H), 2.64 (t, 2 H, J = 7.72 Hz), 1.68-1.26 (m, 20 H), 0.87 (m, 3 H). ^{13}C NMR: δ 145.3, 142.3, 140.3, 134.8, 128.8, 127.5, 126.8, 125.9, 122.8, 122.5, 115.1, 32.3, 32.0, 31.1, 30.9, 30.1, 29.9, 29.7, 27.8, 23.1, 14.5, 14.1, 9.2. HRMS(APCI): calcd for $C_{30}H_{36}S_2$, m/z 460.2258; found, m/z 460.2297.

Conflicts of interest

There are no conflicts to declare.

Acknowledgements

We acknowledge financial support of this work from the Science and Engineering Research Council (Grant 1527200019) of Agency for Science, Technology and Research of Singapore. DFT calculation was supported by the A*STAR Computational Resource Centre through the use of its high performance computing facilities.

.

References

1 P. Foggi, F. V. R. Neuwahl, L. Moroni and P. R. Salvi, *J. Phys. Chem. A*, 2003, **107**, 1689.
2 S. V. Shevyakov, H. Li, R. Muthyala, A. E. Asato, J. C. Croney, D. M. Jameson and R. S. H. Liu, *J. Phys. Chem. A*, 2003, **107**, 3295.
3 F. X. Redl, O. Köthe, K. Röckl, W. Bauer and J. Daub, *J. Macromol. Chem. Phys.*, 2000, **201**, 2091.
4 R. S. H. Liu and A. E. Asato, Journal of Photochemistry and Photobiology C: Photochemistry Reviews, 2003, **4**, 179-194.
5 R. S. H. Liu, *J. Chem. Educ.*, 2002, **79**, 183.
6 M. J. Bearpark, F. Bernardi, S. Clifford, M. Olivucci, M. A. Robb, B. R. Smith and T. Vreven, *J. Am. Chem. Soc.*, 1996, **118**, 169.
7 F. Wang, Y.-H. Lai, N. M. Kocherginsky and Y. Y. Kosteski, *Org. Lett.*, 2003, **5**, 995.
8 H. Xin, C. Ge, X. Yang, H. Gao, X. Yang and X. Gao, *Chem. Sci.*, 2016, **7**, 6701.
9 H. Xin and X. Gao, *ChemPlusChem*, 2017, **82**, 945-956.

View Article Online
DOI: 10.1039/C8TC00895G

10 J.-X. Dong and H.-L. Zhang, *Chinese Chemical Letters*, 2016, **27**, 1097-1104.

11 A. Muranaka, M. Yonehara and M. Uchiyama, *J. Am. Chem. Soc.*, 2010, **132**, 7844.

12 T. Tang, T. Lin, F. Wang and C. He, *Polym. Chem.*, 2014, **5**, 2980.

13 M. Koch, O. Blacque and K. Venkatesan, *J. Mater. Chem. C*, 2013, **1**, 7400.

14 K. Tsurui, M. Murai, S.-Y. Ku, C. J. Hawker and M. J. Robb, *Adv. Funct. Mater.*, 2014, **24**, 7338.

15 S. Ito, A. Nomura, N. Morita, C. Kabuto, H. Kobayashi, S. Maejima, K. Fujimori and M. Yasunami, *J. Org. Chem.*, 2002, **67**, 7295.

16 X. Wang, J. K.-P. Ng, P. Jia, T. Lin, C. M. Cho, J. Xu, X. Lu and C. He, *Macromolecules*, 2009, **42**, 5534.

17 T. Shoji and S. Ito, *Chemistry – A European Journal*, 2017, **23**, 16696-16709.

18 E. Puodziukynaite, H.-W. Wang, J. Lawrence, A. J. Wise, T. P. Russell, M. D. Barnes and T. Emrick, *J. Am. Chem. Soc.*, 2014, **136**, 11043.

19 U. Tomokazu, W. Yusuke, M. Tetsushi and I. Hiroshi, *Chem. Lett.*, 2015, **44**, 47.

20 H. Nishimura, N. Ishida, A. Shimazaki, A. Wakamiya, A. Saeki, L. T. Scott and Y. Murata, *J. Am. Chem. Soc.*, 2015, **137**, 15656-15659.

21 M. Koch, O. Blacque and K. Venkatesan, *Org. Lett.*, 2012, **14**, 1580.

22 Y. Yamaguchi, K. Ogawa, K.-i. Nakayama, Y. Ohba and H. Katagiri, *J. Am. Chem. Soc.*, 2013, **135**, 19095.

23 Y. Yamaguchi, M. Takubo, K. Ogawa, K.-i. Nakayama, T. Koganezawa and H. Katagiri, *J. Am. Chem. Soc.*, 2016, **138**, 11335.

24 I. C.-Y. Hou, V. Shetti, S.-L. Huang, K.-L. Liu, C.-Y. Chao, S.-C. Lin, Y.-J. Lin, L.-Y. Chen and T.-Y. Luh, *Org. Chem. Front.*, 2017, **4**, 773.

25 F. Wang, T. T. Lin, C. He, H. Chi, T. Tang and Y.-H. Lai, *J. Mater. Chem.*, 2012, **22**, 10448.

26 T. Tang, G. Ding, T. Lin, H. Chi, C. Liu, X. Lu, F. Wang and C. He, *Macromol. Rapid Commun.*, 2013, **34**, 431.

27 T. Tang, T. Lin, F. Wang and C. He, *Chem. Commun.*, 2015, **51**, 13229.

28 J. L. Longridge and F. A. Long, *J. Am. Chem. Soc.*, 1968, **90**, 3088.

29 R. A. Gaussian 09, M. J. Frisch, G. W. Trucks, H. B. Schlegel, G. E. Scuseria, M. A. Robb, J. R. Cheeseman, G. Scalmani, V. Barone, G. A. Petersson, H. Nakatsuji, X. Li, M. Caricato, A. Marenich, J. Bloino, B. G. Janesko, R. Gomperts, B. Mennucci, H. P. Hratchian, J. V. Ortiz, A. F. Izmaylov, J. L. Sonnenberg, D. Williams-Young, F. Ding, F. Lipparini, F. Egidi, J. Goings, B. Peng, A. Petrone, T. Henderson, D. Ranasinghe, V. G. Zakrzewski, J. Gao, N. Rega, G. Zheng, W. Liang, M. Hada, M. Ehara, K. Toyota, R. Fukuda, J. Hasegawa, M. Ishida, T. Nakajima, Y. Honda, O. Kitao, H. Nakai, T. Vreven, K. Throssell, J. A. Montgomery, Jr., J. E. Peralta, F. Ogliaro, M. Bearpark, J. J. Heyd, E. Brothers, K. N. Kudin, V. N. Staroverov, T. Keith, R. Kobayashi, J. Normand, K. Raghavachari, A. Rendell, J. C. Burant, S. S. Iyengar, J. Tomasi, M. Cossi, J. M. Millam, M. Klene, C. Adamo, R. Cammi, J. W. Ochterski, R. L. Martin, K. Morokuma, O. Farkas, J. B. Foresman, and D. J. Fox, Gaussian, Inc., *Wallingford CT*, 2016.

30 L. D. Bonifacio, D. P. Puzzo, S. Breslav, B. M. Willey, A. McGeer and G. A. Ozin, *Adv. Mater.*, 2010, **22**, 1351.

View Article Online
DOI: 10.1039/C8TC00895G

TOC

Configurations dependent optical properties and acid susceptibility of azulene compounds

Tao Tang, Tingting Lin, Fuat Erden, FuKe Wang, and Chaobin He

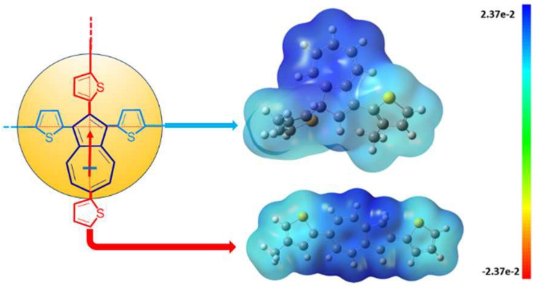

Configurations dependent optical and sensing properties of azulene compounds were achieved simply by change the conjugation directions either along or orthogonally to the dipole direction of azulene. Their application for chemical sensor with sensitivity at ppm level was also demonstrated.